中國機械工程學刊第四十六卷第二期第 153~162 頁(民國一百一十四年)
Journal of the Chinese Society of Mechanical Engineers, Vol.46, No.2, pp 153~162 (2025)

Structural Dynamic Analysis and Topology Optimization of a Propeller Polishing Machine Tool

Shihao Liu*, Jibo Su** and Mao Lin***

Keywords: Propeller; Polishing machine tool; Kinematics analysis; Kinetic analysis; Topology optimization

ABSTRACT

In order to realize automatic polishing of propeller, dynamic analysis and topological optimization of a propeller polishing machine tool were studied. The machine adopts the design of series clamping robot and auxiliary support arm to cooperate, which retains the advantages of high flexibility of series robot, while the addition of auxiliary support arm improves the stiffness of the clamping robot. The spatial coordinate system of the clamping robot of the propeller polishing machine tool was established. The position of the clamping robot in the propeller polishing machine tool was determined using the D-H method, and its working space was calculated using the Montecarlo method. The dynamics analysis of the clamping robot showed that the torque of joint 2 and joint 3 was too large, and the topology optimization of the upper and lower arms of the clamping robot was carried out. According to the topological optimization results, the model of the upper and lower arms was improved, and the structural optimization scheme of the propeller polishing machine tool was finally obtained. The results show that the maximum torque of joint 1, joint 2 and joint 3 is reduced by 13%, 19.6% and 14.8%, respectively.

INTRODUCTIN

Propellers are the core components of ship propulsion systems, and the quality of their surfaces directly impacts the energy conversion efficiency of ships.

Paper Received: July 2024. Revised: September 2024. Accepted November, 2024. Author for Correspondence: Shihao Liu.

* *Professor, School of Mechanical and Electrical Engineering, Hainan University, Haikou 570228, China.*
** *Bachelor, School of Mechanical and Electrical Engineering, Hainan University, Haikou 570228, China.*
****Associate professor, School of Mechanical and Electrical Engineering, Hainan University, Haikou 570228, China.*

Polishing reduces surface roughness and frictional resistance, thereby decreasing drag losses and improving propulsion efficiency. This is crucial for enhancing energy conservation in ships[4]. Furthermore, polishing reduces turbulence and vortices as water or air flows over the propeller, thereby reducing noise and vibration, improving comfort, and decreasing structural fatigue[5]. Polished propellers also extend their service life, reduce maintenance and repair costs, and enhance equipment reliability. In summary, propeller polishing significantly affects overall ship performance, contributing to increased efficiency, reduced transportation costs, improved operational performance, and sustainable development.

Propeller blade surfaces constitute complex free-form surfaces, making them among the most challenging components to manufacture in mechanical production. Currently, both domestic and international propeller manufacturing facilities predominantly employ traditional and relatively outdated manual polishing methods for blade finishing, with limited adoption of fully automated polishing technologies. Manual polishing is inefficient, costly, difficult to maintain consistency and precision, and requires a high level of worker skill. In mass production, manual polishing cannot meet the needs of fast, efficient and accurate processing. Therefore, the development of a propeller CNC polishing machine to achieve automatic polishing operation has become an urgent need in the field of propeller manufacturing.

To solve these problems, some scholars have introduced industrial robots into the polishing process of helicopter blades, mainly including the following methods: using a serial robot for polishing small helicopter blades, using a serial robot combined with a guide rail or a small car for polishing large helicopter blades, using a parallel robot and a mobile platform for polishing helicopter blades, and using a large portal frame for polishing large helicopter blades. XIAO G et al.(2024) proposed a method of high surface integrity string-connected robot sand belt grinding for disk blades with variable inclination force control. Tang Aijun et al.(2022) proposed an intelligent precision polishing and grinding robot, which used a series robot combined with a guide rail for wet polishing, resulting in a 30% increase in polishing efficiency. ZHANG Dianfan et al.(2023) designed a weakly coupled 5-DOF polishing and grinding manipulator with a 2-UPS+(2-UPS)+U parallel mechanism, and analyzed and designed the mechanism of the manipulator. Based on performance evaluation criteria, Monte Carlo method conducted probabilistic analysis of the dimensional parameters of the robotic arm, optimized the parameters based on probabilistic analysis data, and designed a scheme for a weakly coupled 5-DOF parallel robotic arm. In the above method, the stiffness of the series robot is low, and there is a continuous sticking force in the polishing process of the propeller. In the working environment, the series robot with large normal force and small tangential force and insufficient stiffness is difficult to work stably. Although the serial robot stiffness is sufficient, the working space is small and poor flexibility, which is not suitable for the needs of future intelligent factories. Although the gantry frame is suitable for large-scale propeller processing, it has insufficient flexibility and high cost. Therefore, it is necessary to design a flexible and stiff propeller polishing machine tool to meet the needs of the manufacturing industry's transformation to intelligent manufacturing.

Based on the characteristics of propeller polishing and grinding, a propeller polishing machine tool was designed. The focus is on the analysis and design of the clamping robot, using the D-H method for position inverse calculation, and using the Monte Carlo method to draw the total workspace of the clamping robot. Performing dynamic simulation and topology optimization on the clamping robot reduced the weight of the arm and the wrist, and also reduced the maximum torque at the joints. Based on the topology optimized clamping robot, a final design scheme for the helicopter blade polishing machine was obtained.

OVERALL DESIAN OF PROPELLER POLISHING MACHINE TOOL

The Structure Characteristics of Propellers

The structure of a propeller is shown in Figure 1, which consists of a hub and blades. The hub is where the transmission shaft is installed, and it drives the propeller to rotate when working. The blades rotate and push the water or air behind them, generating forward motion. The number of blades on a common propeller is usually 2-6. From the rear of the ship, the observed side of the propeller blade is called the blade face, while the opposite side is known as the blade back. During rotation, the leading edge of the blade is referred to as the leading edge, and the trailing edge is called the trailing edge. The blade root is the part where the blade connects to the hub, and the outer part of the blade is known as the blade tip.

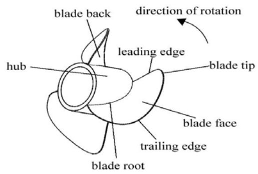

Fig.1 Propeller structure

In a propeller, the surfaces requiring polishing are the blade face and the hub. The blade face, as the primary working surface, demands higher surface quality. The propeller's areas for processing can be divided into the front and back of the blade face and the hub, due to significant structural differences between the blade face and the hub. Using a single polishing device makes it challenging to achieve effective polishing. However, the front and back of the blade face are symmetrical and can be polished using a single polishing device. There are multiple surfaces to be processed on a propeller, so when designing the clamping device, care must be taken to avoid damaging the working surfaces. The spatial structure of propeller blades is complex, with tight spacing between the blades. During the design of a propeller polishing machine tool, particular attention should be paid to interference issues. In summary, the design of the polishing machine not only requires a reasonable mechanical structure, but also needs to take into account the structural features of the propeller itself to improve polishing efficiency and avoid interference.

Structure and Working Principle of propeller polishing machine tool

In order to achieve automatic feeding of the propeller during polishing, the polishing machine uses a serial robot to hold the propeller and complete the polishing operation. At the same time, in order to overcome the problem of insufficient stiffness of the serial robot, a support arm is designed to improve its stiffness. The specific three-dimensional model of the polishing machine is shown in Figure 2. To meet the different polishing requirements of propeller blades and hubs, separate polishing devices were designed: a blade polishing device and a hub polishing device. The blade polishing device is based on a 3-PRS three-degree-of-freedom parallel robot, symmetrically arranged on the machine tool to achieve simultaneous polishing of both sides of the blade. The hub polishing device uses a grinding wheel to polish the hub and blade roots. According to the research on six-axis robots by Zhou Huicheng et al.(2014), a propeller-specific clamping robot was designed, which consisted of a bottom rotary device, a large arm swing device, a small arm swing device, a small arm extension device, a wrist rotary device, a wrist swing device, an end rotary device, and a clamping device. The auxiliary support arm consists of a sliding device, a swing device, an extension device, and a connection device. The clamping robot works in conjunction with auxiliary support arms, which allows the clamping robot to have high flexibility when working alone, and when it works together with the auxiliary support arm, it forms a closed kinematic chain to ensure that the stiffness of the clamping robot during the polishing process meets the requirements.

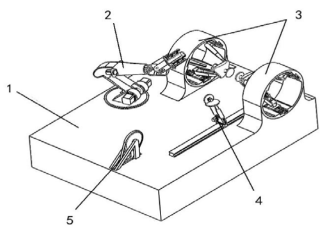

1. Frame 2. Clamping robot 3. Blade polishing device 4. Auxiliary support arm 5. Hub polishing device
Fig.2 propeller polishing machine tool

In the polishing operation, the clamping robot inserts the clamping device into the hub of the propeller, completes the automatic feeding of the propeller for polishing, and then controls the clamping robot to dock with the auxiliary support arm to form a closed kinematic chain. The clamping robot and auxiliary support arm jointly control the propeller to the blade polishing area, where the symmetrical blade polishing device polishes both sides of the blade simultaneously. Then, it moves to the hub polishing device to polish the hub and root of the blade. After polishing is completed, the clamping robot and auxiliary support arm separate, and the clamping robot puts the propeller into the unloading area to complete unloading. The above process is repeated continuously to achieve the polishing of the propeller.

KINEMATIC ANALYSIS OF THE CLAMPING ROBOT

The clamping robot serves as the core working unit for the helicopter blade CNC polishing machine bed, responsible for clamping the helicopter blade and controlling its spatial position and attitude. The position kinematics of the clamping robot is analyzed using the D-H method, and the workspace of the clamping robot is simulated using Matlab, which can provide data support for design to ensure that it meets design requirements.

Position Kinematics

Label the rods in sequence from the base to the end effector: label the base as 0 and the end effector as 7. Rod i, except for the base and end effector, is connected to rods i-1 and i+1 via two joints. The joints are sequentially labeled 1 to 7. Establish a right-handed Cartesian coordinate system {i} on rod i (i.e., the right-handed coordinate system O_i-$X_iY_iZ_i$). The axis Z_i of the coordinate system coincides with the i-th joint axis on link i+1, with its positive direction arbitrarily defined. Except for the base and end effector, draw a perpendicular line from the two joint axis on rod i. The intersection of this line with the axis of the i+1 joint is set as the origin O_i of the coordinate system. The X_i axis coincides with this perpendicular line. The direction from the i-th joint axis towards the i+1-th joint axis is considered the positive direction of the coordinate axis X_i. When the axes of the two joints on rod i are parallel, the X_i axis is perpendicular to both joint axes. When the axes of the two joints on rod i intersect at a point, this intersection point is set as the origin O_i, and the direction of X_i is the same as or opposite to the direction of $Z_{i-1}\times Z_i$. The direction of the Y_i axis in coordinate system {i} is determined by the right-hand rule. Establish a right-handed Cartesian coordinate system {0} on the base (i.e., the right-handed coordinate system O_0-$X_0Y_0Z_0$). The Z_0 axis coincides with the axis of the first joint, the X_0 axis is perpendicular to the Z_0 axis, and the direction of the Y_0 axis is determined by the right-hand rule. Establish a right-handed Cartesian coordinate system {N} on the end effector (i.e., the right-handed coordinate system O_N-$X_NY_NZ_N$), where the X_N axis is perpendicular to the axis of the last (i.e., the Nth) joint, as shown in Figure 3.

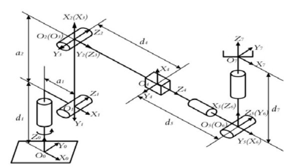

Fig.3 The clamping robot coordinate system

In the D-H convention, the homogeneous transformation matrix (${}^{i-1}A_i$) from coordinate system ({i-1}) to ({i}) is a product of several sub-transformation matrices.

$${}^{i-1}A_i = Trans(Z_{i-1}, d_i)\, Rot(Z_{i-1}, \theta_i)\, Trans(X_i, a_i)\, Rot(X_i, \alpha_i)$$

$$= \begin{bmatrix} \cos\theta_i & -\cos\alpha_i \sin\theta_i & \sin\alpha_i \sin\theta_i & a_i \cos\theta_i \\ \sin\theta_i & \cos\alpha_i \cos\theta_i & -\sin\alpha_i \cos\theta_i & a_i \sin\theta_i \\ 0 & \sin\alpha_i & \cos\alpha_i & d_i \\ 0 & 0 & 0 & 1 \end{bmatrix} \quad (1)$$

For the 7-degree-of-freedom gripper robot described in this paper, the relationship between the end effector and the base coordinate systems is as follows.

$${}^0A_7 = {}^0A_1 {}^1A_2 {}^2A_3 {}^3A_4 {}^4A_5 {}^5A_6 {}^6A_7 = {}^0A_4 {}^4A_7 \quad (2)$$

In the formula

$$\begin{cases} {}^0A_4 = {}^0A_1 {}^1A_2 {}^2A_3 {}^3A_4 \\ {}^4A_7 = {}^4A_5 {}^5A_6 {}^6A_7 \end{cases} \quad (3)$$

According to the three-dimensional model established in SolidWorks and the established coordinate systems, the DH parameters of the clamping robot are determined as shown in Table 1, where a_i is the length of the link, α_i is the twist angle of the link, d_i is the offset between links, θ_i is the rotation angle between links, and JV (joint variable) in the table represents the joint variable.

Tab.1 D-H parameters of clamping robot

Link i	a_i	α_i	d_i	θ_i
1	106	-90	296	θ_1(JV)
2	300	0	0	θ_2(JV)
3	0	-90	0	θ_3(JV)
4	0	0	d4(JV)	0
5	0	90	97.5	θ_5(JV)
6	0	90	0	θ_6(JV)
7	0	0	275	θ_7(JV)

Substituting the parameters from Table 1 into equations (1) and (3), the homogeneous transformation matrix calculated using Matlab is as follows. (For clarity in expression, let sinθ be denoted as sθ and cosθ as cθ):

$${}^0A_4 = \begin{bmatrix} c(\theta_2+\theta_3)c\theta_1 & s\theta_1 & -s(\theta_2+\theta_3)c\theta_1 & c\theta_1(300c\theta_2 - d_4 s(\theta_2+\theta_3) + 106 \\ c(\theta_2+\theta_3)s\theta_1 & -c\theta_1 & -s(\theta_2+\theta_3)s\theta_1 & s\theta_1(300c\theta_2 - d_4 s(\theta_2+\theta_3) + 106 \\ -s(\theta_2+\theta_3) & 0 & -c(\theta_2+\theta_3) & 296 - d_4 c(\theta_2+\theta_3) - 300s\theta_2 \\ 0 & 0 & 0 & 1 \end{bmatrix} \quad (4)$$

$${}^4A_7 = \begin{bmatrix} s\theta_5 s\theta_7 + c\theta_5 c\theta_6 c\theta_7 & c\theta_7 s\theta_5 - c\theta_5 c\theta_6 s\theta_7 & c\theta_5 s\theta_6 & 275c\theta_5 s\theta_6 \\ c\theta_6 c\theta_7 s\theta_5 - c\theta_5 s\theta_7 & -c\theta_5 c\theta_7 - c\theta_6 s\theta_5 s\theta_7 & s\theta_5 s\theta_6 & 275s\theta_5 s\theta_6 \\ c\theta_7 s\theta_6 & -s\theta_6 s\theta_7 & -c\theta_6 & 195/2 - 275c\theta_6 \\ 0 & 0 & 0 & 1 \end{bmatrix} \quad (5)$$

Assuming ${}^0A_7$ is

$${}^0A_7 = \begin{bmatrix} r_{11} & r_{12} & r_{13} & x \\ r_{21} & r_{22} & r_{23} & y \\ r_{31} & r_{32} & r_{33} & z \\ 0 & 0 & 0 & 1 \end{bmatrix} \quad (6)$$

Kinematic Analysis of the Clamping Robot

The workspace of a gripper robot is a collection of all the locations that the robot can reach. As the core part of the propeller CNC polishing machine tool, it is very important to analyze the position that the clamping robot can reach to judge whether the whole machine tool can achieve the expected goal and its performance.The workspace of the robot is usually divided into total workspace, flexible workspace, and sub-workspace. In this paper, only the total workspace is analyzed, which is the maximum space range that the end effector of the clamping robot can reach.

The total workspace of the clamping robot was calculated using the Monte Carlo method. Since the total workspace was only affected by the structural and dimensional parameters of the robot itself, no consideration was needed for the structural and parameter of other parts of the propeller CNC polishing machine bed. By substituting the joint angle values obtained from the positive kinematic equation (6) into the equation, the position coordinates of the end effector can be obtained. Using Matlab to generate random numbers within the specified range, a random position coordinate of the end effector can be generated, and a point in space can be drawn to represent the position. As long as enough random points are generated, the total workspace of the clamping robot can be obtained.

According to the structure and size parameters of the robot, the movement ranges of each link are shown in Table 2 as follows. The specific numerical values of the movement ranges are determined based on the coordinate system established in Figure 3 (θ_i represents the angle of each rotating joint in the coordinate system established in Figure 3, and d_4 is the distance between joint 2 and joint 3, i.e. the total length of link 3 and link 4 (the telescopic link)).

Tab.2 Range of motion of the member

Link i	Range of motion
1	$0 \le \theta_1 \le 2\pi$
2	$-\pi \le \theta_2 \le 0$
3	$-0.25\pi \le \theta_3 \le 0.25\pi$
4	$400mm \le d_4 \le 480mm$
5	$0 \le \theta_5 \le 2\pi$
6	$0.5\pi \le \theta_6 \le 1.5\pi$
7	$0 \le \theta_7 \le 2\pi$

Based on the specified range of motion, the rand() function in Matlab was used to randomly generate values within the range defined in Table 2. According to equation (2), (4), (5) and random generated values, the randomly generated end-effector coordinates were obtained. Matlab was utilized to plot the obtained coordinates as a three-dimensional scatter plot. This scatter plot allowed visualization of the total workspace of the clamping robot. Through experimentation, it was found that using 9000 points provides the most intuitive scatter plot, as shown in Figure 4.

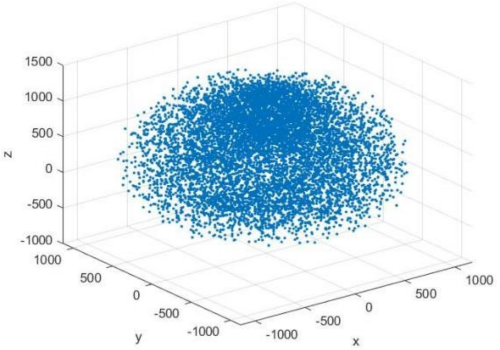

Fig.4 Scatter diagram of the working space of the robot arm

DYNAMIC SIMULATION OF CLAMPING ROBOT

In order to analyze the force distribution at each joint of the clamping robot for subsequent optimization and design improvements, the three-dimensional parametric model of the clamping robot, established in SolidWorks software, was imported into Adams software for dynamic simulation analysis, as shown in Figure 5. In order to simplify the analysis of multi-body dynamics model, the structure of motor, gear, transmission rod and screw nut in the model was removed, and the material and motion pair were added. Due to the complex structure of the model, the kinematic relationship between joints was difficult to analyze, so the compensation factor γ=0.7 was defined and the simulated power was modified.

Fig.5 Multi-body dynamics model of clamping robot

According to the expected working path, the working parameters of each joint are defined as shown in Table 3.

Tab.3 Operating parameters of joints

Joints	0-4s	4-5s	5-10s	10-15s
1	120°	0	-120°	-30°
2	-60°	0	60°	-30°
3	-30°	0	30°	-30°
4	-80mm	0	80mm	-80mm
5	0	0	0	49.11°
6	-60°	0	60°	41.44°

Joint 4 is a translational joint, while the other joints are rotational joints. Control of each joint was implemented using the STEP function in Adams, with the function plot of STEP(time, 0, 0, 15, 10) shown in Figure 6.

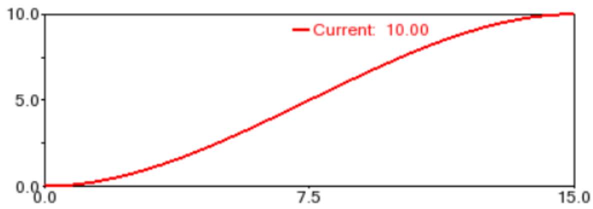

Fig.6 STEP function image

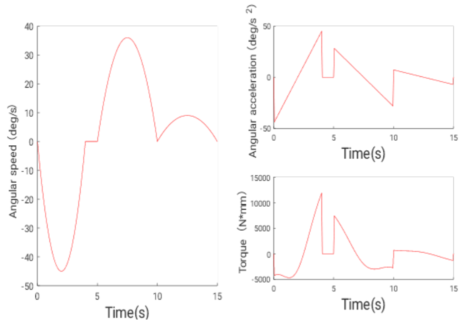

a. Simulation results of joint 1

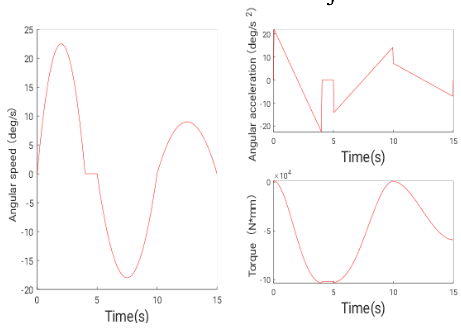

b. Simulation results of joint 2

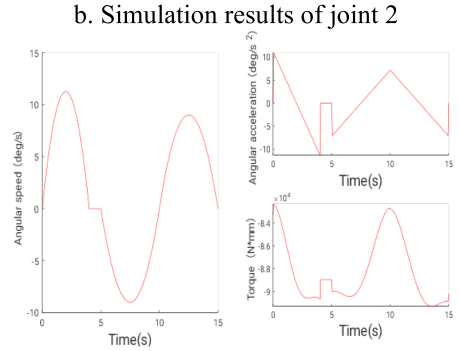

c. Simulation results of joint 3

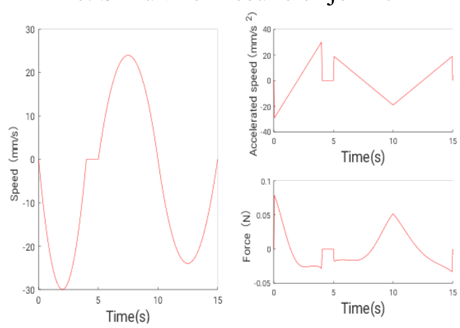

d. Simulation results of joint 4

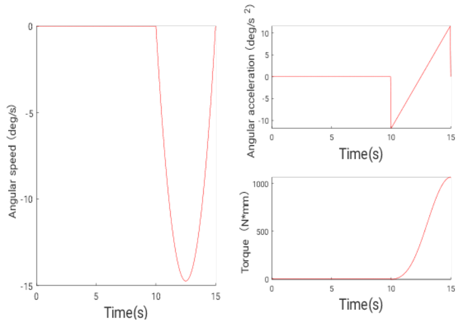

e. Simulation results of joint 5

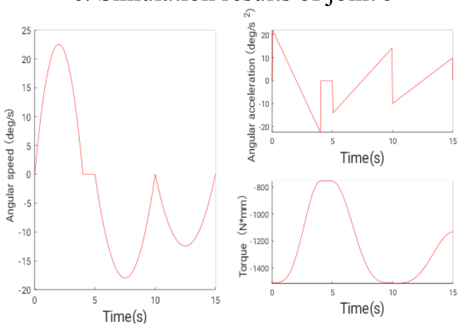

f. Simulation results of joint 6

Fig.7 Motion regularity of each joint of clamping robot

Based on the Adams simulation results, the minimum torque and power required to drive each joint can be estimated, as shown in Table 4.

The power calculation formula is as follows.

$$P = T\omega \tag{7}$$

Angular velocity and torque data were exported from Adams. Matlab was used to extract speed and torque data, which were multiplied together, and the absolute value and the maximum value was taken to obtained the calculated minimum power. The estimated minimum power was obtained by dividing the calculated minimum power by the compensation factor γ.

Tab.4 Minimum power and maximum torque of joints

Joints	The calculated minimum power（W）	The estimated minimum power（W）	The maximum torque（N·m）
1	192.6444	275.21	11.897
2	1657.7	2368.2	103.5
3	1006	1437.1	91.298
5	6.6	9.4	0.58
6	30.5	43.6	1.5

From the data in the table above, it can be observed that the maximum torque for Joint 2 and Joint 3 are significantly higher than for the other joints. Excessive torque is detrimental to the long-term stable operation of the clamping robot. The reason for the higher maximum torque in Joints 2 and 3 compared to Joint 1 is the weight of the upper and lower arms. Therefore, the next step will focus on addressing this issue.

TOPOLOGY OPTIMIZATION OF THE CLAMPING ROBOT

To address the issue of excessive torque identified in joints 2 and 3 during simulation, topology optimization using the topology optimization feature in the Comsol optimization module was applied to optimize the upper and lower arms of the clamping robot. This optimization aimed to maximize stiffness while reducing material usage, thereby lightening the load on the motors.

Topology Optimization of the Lower Arm

The lower arm is a key component that connects the main body and the end effector of the robot and is responsible for transmitting power and attitude control. The lightweight design of the forearm is very important, which can reduce the overall load of the clamping robot, reduce the joint force, and improve the motion speed and accuracy.

A projection of the lower arm model created in SolidWorks was used to establish a simplified 2D simulation model in Comsol, as shown in Figure 8. The model was segmented into regions. The blue area was the optimized area, and the gray area was the non-optimized area.

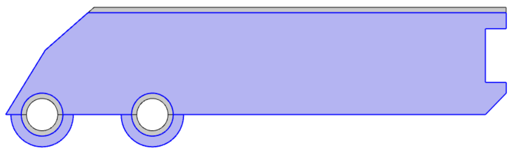

Fig.8 Forearm simulation model

In the global definition, Structural Steel was added as the material. The topology optimization-density model was Integrated into the component, linking it topologically with the materials within the component. The loading and constraints of the lower arm were simplified and them integrated into the model. The mesh was divided into free quadrilateral elements, sized as "fine". Topology optimization was applied into the study, aiming to minimize the total elastic strain energy as the objective function. The constraint was set with a maximum value of 0.6 for the average material volume fraction θ. The number of iterations was set to 410, and the lower bound filter was set to 0.45, with results shown in Figure 9.

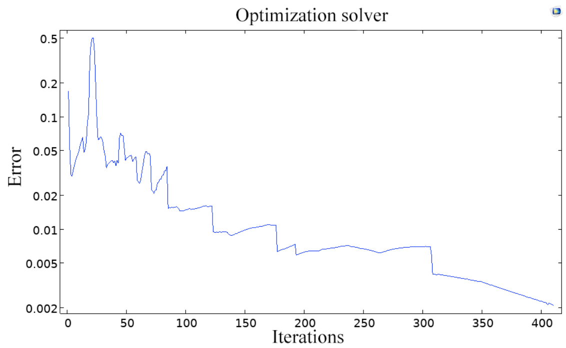

a. Convergence graph of the lower arm topology optimization

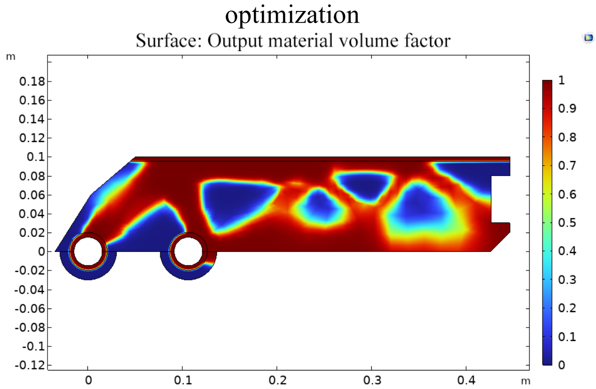

b. The lower arm output material volume factor

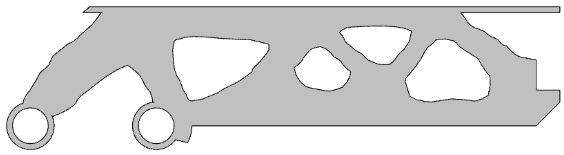

c. Result after filtering

Fig.9 The lower arm topology optimization results

Based on the topology optimization results and the structural requirements of the lower arm, the three-dimensional model of the lower arm was established as shown in Figure 10. The central cavity was designed for gear installation, with the gearbox casing covering the cavity to achieve enclosed gear transmission. The remaining sections were thinned to ensure enclosed gear transmission, with a smooth cylindrical surface at the front end, which was not within the scope of topology optimization. This section was designed for wrist extension and retraction, with internal support for gears and transmission shafts.

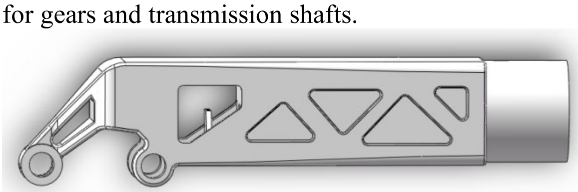

Fig.10 Optimized the lower arm model

Topology Optimization of the Upper Arm

The upper arm bears the majority of the robot's mass and is one of the larger components in the entire robot. Its rigidity is closely related to the overall rigidity of the clamping robot. If the rigidity is insufficient and the end is disturbed, significant torque may occur on the upper arm. Therefore, topology optimization of the upper arm is conducted to reduce the mass of the clamping robot while maintaining stiffness.

Based on the previously established 3D model, a 2D simulation model was generated in Comsol as shown in Figure 11. The blue area was the optimized area, and the gray area was the non-optimized area.

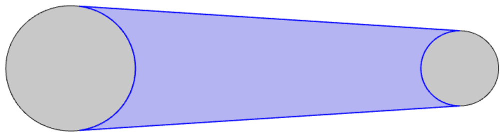

Fig.11 The upper arm simulation model

Similar to the optimization steps for the lower arm, dividing the mesh uniformly across the entire area leads to poor density in dense points. Therefore, the circular area on the left was separately meshed. The objective function was set to the total elastic strain energy minimization, with the average material volume fraction θ was set to 0.6. The optimization was carried out over 400 iterations, with the lower bound filter set to 0.45. The optimization results are shown in Figure 12.

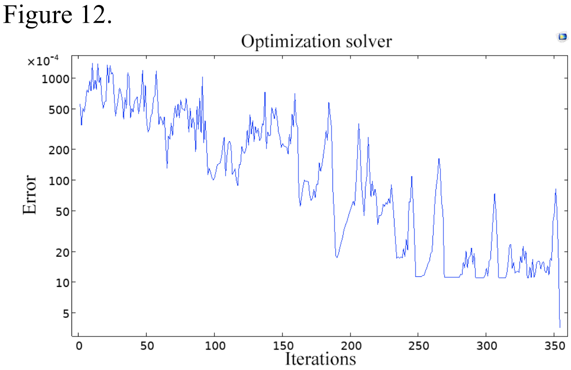

a. The upper arm topology optimization convergence graph

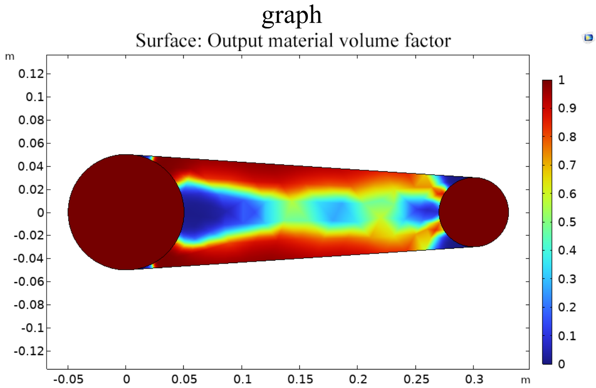

b. The upper arm output material volume factor

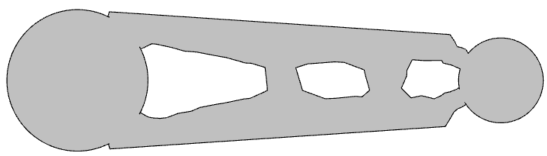

c. Result after filtering
Fig.12 Topology optimization results of the upper arm

According to the topology optimization results and considering the original structure of the robot, the optimized upper arm is shown in Figure 13. The optimization of the 3D model primarily focuses on three void structures. Due to the absence of an internal transmission system, it is directly hollowed out. Both ends are left unoptimized for ease of machining.

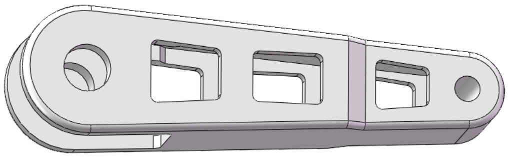

Fig.13 The optimized large arm model

Simulation Results after Optimization

Based on the results of the topology optimization, modifications were made to the clamping robot model in SolidWorks. The updated 3D model was imported into Adams, as shown in Figure 14, where material properties and motion joints were incorporated into the multi-body dynamics model.

Fig.14 The optimized multi-body dynamics model

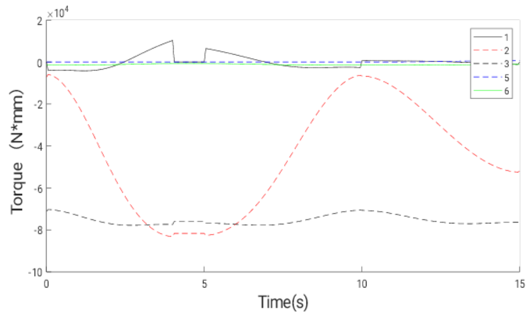

Fig.15 The torque of each joint after optimizing

According to the simulation based on the operating parameters in Table 3, the optimized torque values for each joint are shown in Figure 15. Table 5 presents the maximum torques for each joint and their respective improvement rates, excluding discussion on Joint 4, which involves linear motion.

Tab.5 Maximum torque and improvement rate of joints

Joints	Original maximum torque （N·m）	Improved maximum torque （N·m）	Improvement rate
1	11.897	10.35	13%
2	103.5	83.19	19.6%
3	91.298	77.79	14.8%
5	0.58	0.58	0%
6	1.5	1.5	0%

According to the simulation results, it is evident that except for Joints 5 and 6, the maximum torques experienced by the other rotating joints have decreased. Specifically, Joint 1, Joint 2, and Joint 3 saw reductions of 13%, 19.6%, and 14.8% in their maximum torques during the simulation process.

Results Analysis

After topological optimization of the upper and lower arms of the clamping robot, not only the total weight is reduced, but also the burden of joint 1 to joint 3 is reduced, and the material use and design efficiency are optimized. This optimization scheme provides an effective path for lightweight and torque optimization of series robots. By optimizing the topological structure of the propeller polishing machine tool, the effectiveness of the optimization algorithm in robot design is verified, and the further application of the optimization algorithm in robot design is promoted, which provides case support for Comsol multi-objective optimization problem and enriches the theory of mechanical design optimization. The improved robot not only improves dynamic performance and polishing accuracy, but also reduces joint torque, reducing motor power and energy consumption, in line with the concept of green design and sustainable development.

CONCEPTUAL DESIGN OF APPLICATION SCENARIOS

Currently, manual polishing remains predominant for most propellers. Existing propeller polishing machine tools often employ robotic arms with polishing heads for this task, which suffer from low stiffness and difficulty achieving fully automated operations.

The polishing machine designed in this paper not only polishes both the propeller blades and hub but also facilitates automated loading and unloading of propellers, as illustrated in Figure 16.

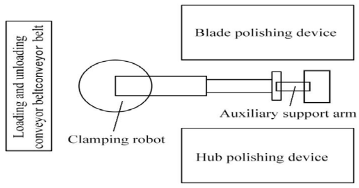

Fig.16 Simplified polishing machine schematic

The CNC propeller polishing machine tool is installed in front of the loading and unloading conveyor belt. The clamping robot grips the propeller to be polished for automated loading. During the polishing process, the clamping robot docks with the auxiliary support arm (as shown in Figure 17) to ensure stability of the propeller.For polishing the propeller blades, the clamping device is positioned vertically with respect to the ground. The motor on the auxiliary support arm rotates the propeller during the polishing process conducted by the blade polishing device.When polishing the hub, the clamping device is positioned at a certain angle with respect to the ground to complete the hub polishing.After polishing, the clamping robot separates from the auxiliary support arm and places the propeller onto the loading and unloading conveyor belt for unloading.

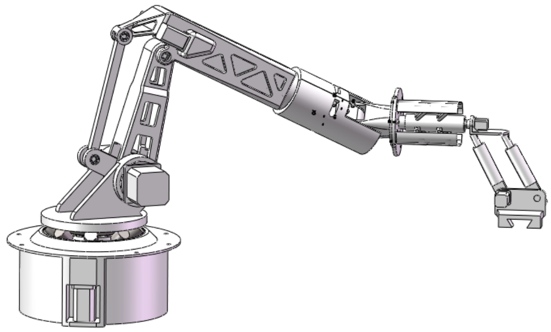

Fig.17 Docking diagram of clamping robot

Compared to existing propeller polishing machine tools, this CNC propeller polishing machine tool can autonomously complete the entire process of propeller polishing without requiring human intervention. The entire polishing process is automated and holds promise for playing a crucial role in future smart factories.

CONCLUSION

Aiming at a propeller polishing machine, a symmetrical blade polishing device and a hub polishing device based on grinding wheel are designed, and an auxiliary support arm is proposed. This design not only retains the flexibility of the series robot, but also significantly enhances the rigidity, enabling the clamping robot to efficiently perform loading and unloading operations, laying the foundation for intelligent design.

The combination of the symmetrical blade polishing device and the wheel hub polishing device, as well as the introduction of auxiliary support arms, these improvements improve the stability and efficiency of the robot operation. The D-H method is used to draw the space coordinate system, and the accurate position solution is carried out, and the Monte Carlo method is used to calculate the working space, which ensures the comprehensiveness of the design. At the same time, we used Adams software for dynamic simulation analysis, and Comsol software for topology optimization, which significantly reduced the maximum torque of joint 2 and joint 3, improved the overall performance and reduced the cost.

However, the rigidity and stability of the current design under extreme operating conditions still need to be further verified. In addition, while optimization improves performance, the impact on other key components needs to be fully evaluated. Future work should focus on improving the robustness and adaptability of the design, exploring its performance in a wider range of application scenarios, and optimizing for problems in actual operation to promote the implementation of intelligent design. This will include consideration of more operational variables and verification of compatibility with actual production environments.

DECLARATION OF CONFLICTING INTERESTS

The author(s) declared no potential conflicts of interest with respect to the research, authorship, and/or publication of this article.

DATA AVAILABILITY

The data that support the findings of this study are available from the corresponding author upon reasonable request.

ACKNOWLEDGEMENTS

This work was supported by the National Natural Science Foundation of China (Grant No. 52365032) .

REFERENCES

Cooke J P, Campbell M F, Steager E B, et al. Numerical and experimental study on the addition of surface roughness to micro-propellers[J]. Physics of Fluids, 2023, 35(11).

HOU L, ZHANG L, Kim J. Energy Modeling and Power

Measurement for Mobile Robots[J]. Energies, 2019,12(1): 27.
IBARAKI S, FUKUDA K, ALAM M, et al. Novel six-axis robot kinematic model with axis-to-axis crosstalk[J]. CIRP Annals - Manufacturing Technology, 2021,70(1):411-414.
JI Yangyang, TIAN Guizhong, ZHOU Honggen. Development and present situation of the marine propeller advanced manufacturing technology [J]. Ship Sci-ence and Technology,2015,37(05):9-15.
LIU Shihao, HUANG Pengfei, WANG Fei, et al. Structure design and functional analysis of propeller CNC polishing machines[J]. Manufacturing Technology & Machine Tool, 2022,(04):38-42.
LI Xingchen, YANG Guoqing, WANG Xian, et al. Fast Solution of 6-axis Industrial Robot Workspace [J]. Mechanical Science and Technology for Aerospace Engineering,2023,42(08):1213-1220.
LI Y, XU Q. Kinematics and inverse dynamics analysis for a general 3-PRS spatial parallel mechanism [J]. Robotica, 2005,23(2):219-229.
Majumder P, Maity S. A critical review of different works on marine propellers over the last three decades[J]. Ships and Offshore Structures, 2023, 18(3): 391-413.
SUN L, LIANG F, FANG L. Design and performance analysis of an industrial robot arm for robotic drilling process[J]. The Industrial Robot, 2019, 46(1):7-16.
TANG Aijun, HUAN Yanli, HU Yane,et al. Development and Application of Intelligent Precision Polishing Robot[J]. Mechanical & Electrical Engineering Technology, 2022,51(11): 127-130.
Rodrigues A F G. Development of a Propeller Blade for a Variable Pitch Mechanism[D]. Universidade da Beira Interior (Portugal), 2022.
WANG Fei, ZHAO Xun, QI Xiaohai, et al. A Research Progress in Ship Noise Control Technology [J]. Naval Architecture and Ocean Engineering, 2024, 40(02):7-14.
WANG R, GE Y, GUO X. Investigation on Tool Path Planning Algorithm of Propeller Blade Double-Sided Collaborative Machining[J]. Applied Sciences, 2023, 13(11):6529.
WANG Xi, ZHAO Chongnian, WANG Wenqiang. Topology Optimization and Joint Simulation Based on COMSOL[J]. Equipment Manufacturing Technology, 2019, (09):171-174.
Wang Z, Lin X, Shi Y, et al. Reducing roughness of freeform surface through tool orientation optimization in multi-axis polishing of blisk[J]. The International Journal of Advanced Manufacturing Technology, 2020, 108: 917-929.
XIAO G, LIU X, SONG K, et al. Research on robotic belt grinding method of blisk for obtaining high surface integrity features with variable inclination angle force control[J]. Robotics and Computer-Integrated Manufacturing, 2024,86
XIAO Y, WANG J, YANG J, et al. Dynamic simulation research of adaptive support mechanism of pipeline inspection robot based on ADAMS[J]. Journal of Physics: Conference Series,2023,2450(1):012047.
XU Z, ZHAO Y, XIAN L, et al. Workspace Solution and Space Trajectory Planning of 5-DOF Manipulator[J]. Journal of Physics: Conference Series, 2022, 2239(1): 012015.
YOUN J , JUN Y , PARK S. Interference-free tool path generation in five-axis machining of a marine propeller[J]. International Journal of Production Research, 2003,41(18):4383-4402.
Zhang B, Wu S, Wang D, et al. A review of surface quality control technology for robotic abrasive belt grinding of aero-engine blades[J]. Measurement, 2023: 113381.
ZHANG Dianfan, DAI Shijie, LI Hongxiu,et al. Design of a 5-DOF Weak Coupling Polishing Manipulator[J]. Machinery Design & Manufacture, 2023, (02): 259-265.
ZHANG H, LU W, WU C, et al. Velocity optimization algorithm of 4-DOF robot end-effectors[J]. Cluster Computing,2019,22(3s):6305-6314.
ZHANG L, MENG X, DING Z, et al. Simulation-Based Reliability Design Optimization Method for Industrial Robot Structural Design[J]. Applied Sciences, 2023, 13(6):3776-3776
ZHAO Y, LI H, LI Z, et al. Kinematics and Dynamics Simulation of Lower Limb Exoskeleton Walking Assist Mechanism[J]. Journal of Physics: Conference Series, 2023,2528(1):012052.
ZHOU Huicheng, REN Zengjun. Mechanical Design and Dynamic Analysis of Six-DOF Robot[J]. Machine Tool & Hydraulics, 2014,42(09):1-5

螺旋槳拋光機床結構動態分析及拓撲優化

劉世豪 蘇紀博 林茂
海南大學機電工程學院

摘要

為了實現螺旋槳的自動拋磨加工，對一種螺旋槳拋光機床進行動態分析和拓撲優化研究。該機床採用串聯夾持機器人與輔助支撐臂協同配合的設計，保留了串聯機器人靈活性高優點的同時，輔助支撐臂的加入又讓夾持機器人的剛度得到了提高。建立螺旋槳拋光機床夾持機器人的空間坐標系，用 D-H 方法對夾持機器人進行位置正解，並用蒙特卡羅法計算了夾持機器人的工作空間。對夾持機器人進行了動力學分析，發現關節2與關節3轉矩過大，並對夾持機器人的大臂和小臂進行拓撲優化。根據拓撲優化結果對大臂和小臂的模型進行改進，最終得到了螺旋槳拋光機床的結構優化方案。對優化的螺旋槳拋光機床再次進行動力學分析，結果表明關節1、關節2與關節3 所承受的最大轉矩分別減少 13%、19.6%和 14.8%。